Journal of Materials Chemistry C

RSC Publishing

PAPER

View Article Online
View Journal | View Issue

Cite this: J. Mater. Chem. C, 2013, 1, 7568

Evaluating the potential for high thermoelectric efficiency of silver selenide†

Tristan Day,[a] Fivos Drymiotis,[a] Tiansong Zhang,[b] Daniel Rhodes,[c] Xun Shi,[b] Lidong Chen[b] and G. Jeffrey Snyder*[a]

Received 12th September 2013
Accepted 11th October 2013

DOI: 10.1039/c3tc31810a

www.rsc.org/MaterialsC

Measurements and modeling of electronic transport properties of n-type $Ag_{2+x}Se$ suggest that this material could have a thermoelectric figure of merit zT greater than 1 at 300 K and above. The exceptional performance can be traced to the exceptionally high mobility, higher than other optimized thermoelectric materials. Although zT decreases at high temperature because of a transition to a phase with high carrier concentration, our model indicates that reducing the carrier concentration will lead to high thermoelectric performance at room temperature for cooling applications as well as up to 600 K for waste heat recovery.

1 Introduction

Thermoelectric materials, which convert a temperature difference into a voltage, or act as sources and sinks of heat upon application of an electric current, show promise as efficient harvesters of waste heat from industrial facilities or automobile exhaust, and as an alternative means of refrigeration and cooling. The advantages of thermoelectrics over vapor-compression cooling systems include greater reliability and freedom from vibration due to solid-state operation, and reduced size. Additionally, thermoelectrics do not use greenhouse gas refrigerants.[1]

Increasing the efficiency of a thermoelectric material necessitates increasing the figure of merit, zT. zT is equal to $S^2T\rho^{-1}\kappa^{-1}$, where S is the Seebeck coefficient, T is the absolute temperature, ρ is the electrical resistivity, and κ is the total thermal conductivity. κ is the sum of a lattice contribution and an electronic contribution. Thermoelectric materials used in practice have zT near 1.

One widely studied class of thermoelectric materials is the chalcogenide compounds. These include such materials as PbTe,[2] alloys of PbTe and $AgSbTe_2$, called LAST materials,[3] alloys of GeTe and $AgSbTe_2$, called TAGS materials,[4] and Bi_2Te_3.[5] Chalcogenides are good thermoelectric materials because they have high electrical conductivity and low thermal conductivity.

The n-type chalcogenide $Ag_{2+x}Se$ has promising thermoelectric properties, but only a handful of studies have been conducted on it. Previous investigations on $Ag_{2+x}Se$ report that it has high electrical conductivity and low thermal conductivity and that its zT approaches 1 at room temperature.[6,7] Lower zT values have been reported in mechanically-alloyed silver selenide.[8] The reported zT increases as temperature increases from 70 K to room temperature.[7] This is especially encouraging because $Ag_{2+x}Se$ becomes a superionic conductor around 407 K,[9] as does Cu_2Se, which has been reported to have a zT that increases with temperature to 1.5 at 1000 K.[10] Cu_2Se has a low lattice thermal conductivity because the mobile Cu ions scatter phonons, an effect also seen in Ag ion conducting $AgCrSe_2$.[11] Considering the previously reported zT behavior and the mobile Ag ions, $Ag_{2+x}Se$ could have high zT in the superionic phase. The authors of the previous work on $Ag_{2+x}Se$ made no attempt to optimize its thermoelectric properties, suggesting that the already good thermoelectric performance of this material could be made even better. An additional feature of $Ag_{2+x}Se$ is the abundance of its elements in the Earth's crust compared to Bi_2Te_3, a thermoelectric in wide use for cooling applications.[12]

While $Ag_{2+x}Se$ appears to be a good thermoelectric material, there is some discrepancy in the reported room temperature zT values. The reported zT at room temperature varies from 0.32 to 0.96.[6,7] Furthermore, these reports contain no measurements of the thermoelectric properties above room temperature. It seems possible that $Ag_{2+x}Se$ could be a useful thermoelectric material. However in order to confirm this we must know how to control zT and the value of the maximum possible zT.

In this work we measure the properties of $Ag_{2+x}Se$ from 300 K to 673 K and propose a model relating the maximum zT at room temperature and above to the Hall carrier concentration. We use a single parabolic band (SPB) model to analyze our measurements and establish the mechanism for obtaining high

[a]Materials Science, California Institute of Technology, Pasadena, California, 91106, USA. E-mail: jsnyder@caltech.edu

[b]CAS Key Laboratory of Energy-conversion Materials, Shanghai Institute of Ceramics, Chinese Academy of Sciences, Shanghai, 200050, China

[c]National High Magnetic Field Laboratory, Florida State University, Tallahassee, Florida, 32310, USA

† Electronic supplementary information (ESI) available. See DOI: 10.1039/c3tc31810a

zT. We show that if the Hall carrier concentration were carefully controlled to 1–2 $\times$ 10^{18} cm^{-3} (significantly lower than usually achieved), a zT of 1 at 300 K and above could be possible.

2 Results and discussion

A variety of compositions of $Ag_{2+x}Se$ were prepared from ingots created by direct fusion of the elements and by hot-pressing $Ag_{2+x}Se$ powders. The details of our synthesis are in the Experimental section.

It is well known that carrier concentration controls thermoelectric properties. Therefore, we begin our discussion of the results with the Hall carrier concentration as a function of temperature, shown in Fig. 1(a). The curves are differentiated by their room temperature Hall carrier concentrations. The Hall carrier concentration rises then jumps to 3–5 $\times$ 10^{19} cm^{-3} at the superionic phase transition temperature, measured by differential scanning calorimetry to be 407 K. Above the phase transition, the samples labeled n_H = 5.56E18and n_H = 4.97E18 (Fig. 1(a), blue and black squares, respectively) exhibit the beginning of an increase in the Hall carrier concentration around 600 K; the concurrent decrease in the Seebeck coefficient of these samples at that temperature suggests that the additional carriers are holes. Fang *et al.*, using LDA, found a pseudo-gap structure in stoichiometric Ag_2Se.[13] Improved exchange-correlation potentials will most likely open up a gap, which could then explain the observed transport properties.

The Hall carrier concentration as a function of the nominal Ag excess is given in Table 1. However, it is difficult to establish a correlation between the Ag content and the Hall carrier concentration because the actual average Ag content in the matrix phase may differ from the nominal due to the presence of small amounts of impurity phases, *e.g.* Ag in the grain boundaries. This could be exacerbated due to Ag ion movement

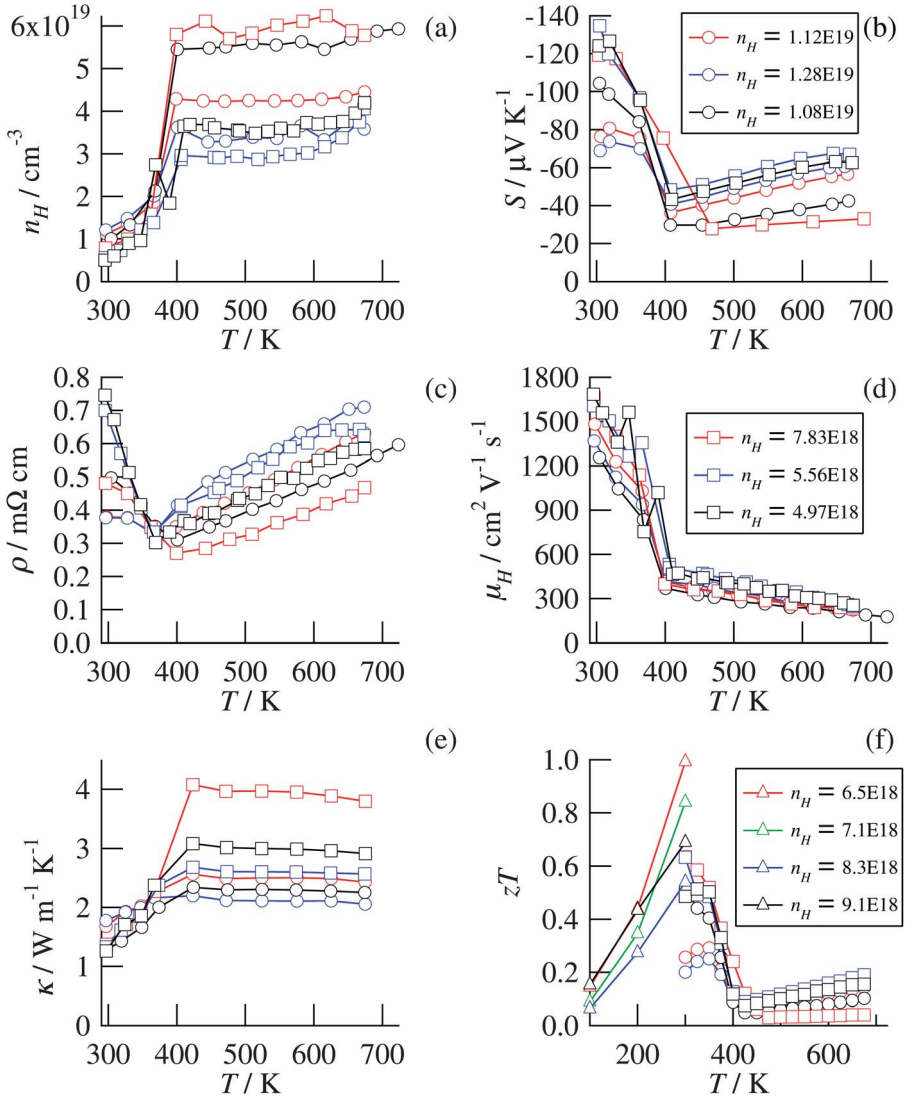

Fig. 1 Transport properties of $Ag_{2+x}Se$. Circles represent hot-pressed samples, squares represent samples cut from ingots, and triangles are from Aliev.[7] The legends for all figures are shown in (b) and (d). Samples are identified by their room temperature n_H values in units of cm^{-3}. Only heating curves are shown. Cooling curves can be found in Fig S3 and S4.†

Table 1 Hall carrier concentrations at 300 K

Nominal composition	Hot-pressed/ 10^{18} cm^{-3}	Ingot/ 10^{18} cm^{-3}
Ag_2Se	11.2	7.83
$Ag_{2.0006}Se$	12.8	5.56
$Ag_{2.0027}Se$	10.8	4.97

during ingot consolidation and hot-pressing. These results present two challenges. First, it is difficult to establish a correlation between the carrier concentration and the Ag content. Second, hot-pressing seems to increase the carrier concentration. Since it is the Hall carrier concentration that controls the thermoelectric performance, it would be best to determine the doping mechanism; however this is beyond the scope of this work.

Assuming it were possible to control the carrier concentration in $Ag_{2+x}Se$, we can estimate the maximum possible zT at any temperature after we estimate the electron effective mass m^*, the mobility parameter μ_0, and the lattice thermal conductivity κ_l. We will estimate these parameters at 300 K, the temperature at which the highest zT in this material has been reported. Because the Hall carrier concentration behavior differs so dramatically above and below the phase transition, we will model the transport properties in each region separately. In our analysis, we use the single parabolic band (SPB) model as a first approximation for the conduction band as is commonly done to derive the density of states effective mass m^*. This formulation ignores the valence band as if it were completely filled and assumes that holes do not contribute to conduction. The exact formulas used are derived for when the electron mobility is limited by acoustic phonon scattering, which will be discussed later. The mathematical details of this model are given in the ESI.†

The trend of the Seebeck coefficient with temperature, shown in Fig. 1(b), can be explained by the behavior of the Hall carrier concentrations of the samples. The Seebeck coefficient drops from −70 to −140 μV K^{-1} at 300 K to −30 to −50 μV K^{-1} at 407 K for all samples regardless of starting composition and processing method. The Hall carrier concentration is a dramatically increasing function of temperature in this region, which can explain the decrease in the Seebeck coefficient. Above the phase transition, where the Hall carrier concentration is relatively constant, the Seebeck coefficient increases with temperature, as expected for materials that can be approximated by a single parabolic band.[14] The Seebeck coefficients of the samples labeled $n_H = 5.56E18$ and $n_H = 4.97E18$ (Fig. 1(b), blue and black squares) stop increasing around 650 K, concurrent with an observed increase in Hall carrier concentration, which is likely due to the thermal excitation of minority carriers.

We used the n_H and S data (Fig. 2(a)) to estimate the electron effective mass m^*. The plot includes data from other studies in order to get a more representative value of m^*.[6,7] While hysteresis between heating and cooling curves (Fig. S3 and S4†), sample inhomogeneity, and measurement instability add uncertainty to our estimate of m^*, the obvious trend seen in Fig. 2(a) yields an m^* of 0.2 m_e below the phase transition and 0.3 m_e above the phase transition. These values are comparable to those calculated by Fang, *et al.*[13]

The changing Hall carrier concentration can also explain the trend of the resistivity with temperature, shown in Fig. 1(c). The resistivity drops from 0.4–0.7 mΩ cm at 300 K to ~0.3 mΩ cm at 407 K. The resistivities of two samples (Fig. 1(c), blue and black squares) roll off to a constant value around 600 K in agreement with the increasing Hall carrier concentration. In the other samples above the phase transition, the resistivity increases with temperature typical of heavily doped semiconductors, due to a decrease in Hall mobility, shown in Fig. 1(d).

A Hall mobility limited by acoustic phonon scattering will follow a T^{-p} power law, with the value of p greater than 0.5.[15] The absolute values of the slopes of the curves in Fig. S5† are all greater than 0.5, indicating that acoustic phonons are the dominant scatterers of electrons. There is also a drop in Hall mobility across the superionic transition. This could be because in superionic $Ag_{2+x}Se$, the Ag ions move freely and tend to scatter electrons more efficiently than a static lattice.

We estimated the mobility parameter μ_0 from the Hall mobility and Hall carrier concentration data. The mobility Pisarenko plot is shown in Fig. 2(b). We estimate a μ_0 of 2800 cm^2 V^{-1} s^{-1} below the phase transition and 1800 cm^2 V^{-1} s^{-1} above the phase transition. The Hall mobilities from Aliev[7] (as high as 6100 cm^2 V^{-1} s^{-1}) and Ferhat[6] (as high as 11 610 cm^2 V^{-1} s^{-1}) are not shown in Fig. 2(b) because they are much greater than the values in this study; we were not able to reproduce these high mobility values despite synthesizing and measuring a large number of samples of $Ag_{2+x}Se$.

The predicted mobility at room temperature and the optimum carrier concentration is much greater than that for other n-type thermoelectric materials. At the optimum carrier concentration of 1.6×10^{18} cm^{-3}, we predict that $Ag_{2+x}Se$ will have a Hall mobility of 2200 cm^2 V^{-1} s^{-1} at 300 K. At their respective optimum carrier concentrations, I-doped PbTe has a Hall mobility of 1100 cm^2 V^{-1} s^{-1},[16] Te-doped Bi_2Te_3, 212 cm^2 V^{-1} s^{-1},[5] $La_{3-x}Te_4$, 4 cm^2 V^{-1} s^{-1},[17] and n-type $CoSb_3$ has a mobility of 41.2 cm^2 V^{-1} s^{-1}.[18] The large value of the Hall mobility in $Ag_{2+x}Se$ is due to the low effective mass and is the cause of the low optimal carrier concentration. As μ_0 increases, the β parameter increases, which in turn reduces the optimal carrier concentration.[16]

The total thermal conductivity κ (shown in Fig. 1(e)) is typically considered as containing a lattice contribution κ_l and an electronic portion κ_e. The electronic portion is equal to LT/ρ, where L is the Lorenz number (computed from Eqn. S(11)†), T is absolute temperature, and ρ is the resistivity. For $Ag_{2+x}Se$, the electronic portion of the thermal conductivity constitutes 70% to 80% of the total thermal conductivity between 300 K and 400 K, as computed from the resistivity values in that region and the estimated Lorenz number, discussed below; hence, the electronic portion dominates the total thermal conductivity in that temperature region. κ increases from ~1.5 W m^{-1} K^{-1} at 300 K to 2–4 W m^{-1} K^{-1} above the phase transition. Consequently, the increase in κ is driven by the decrease in the

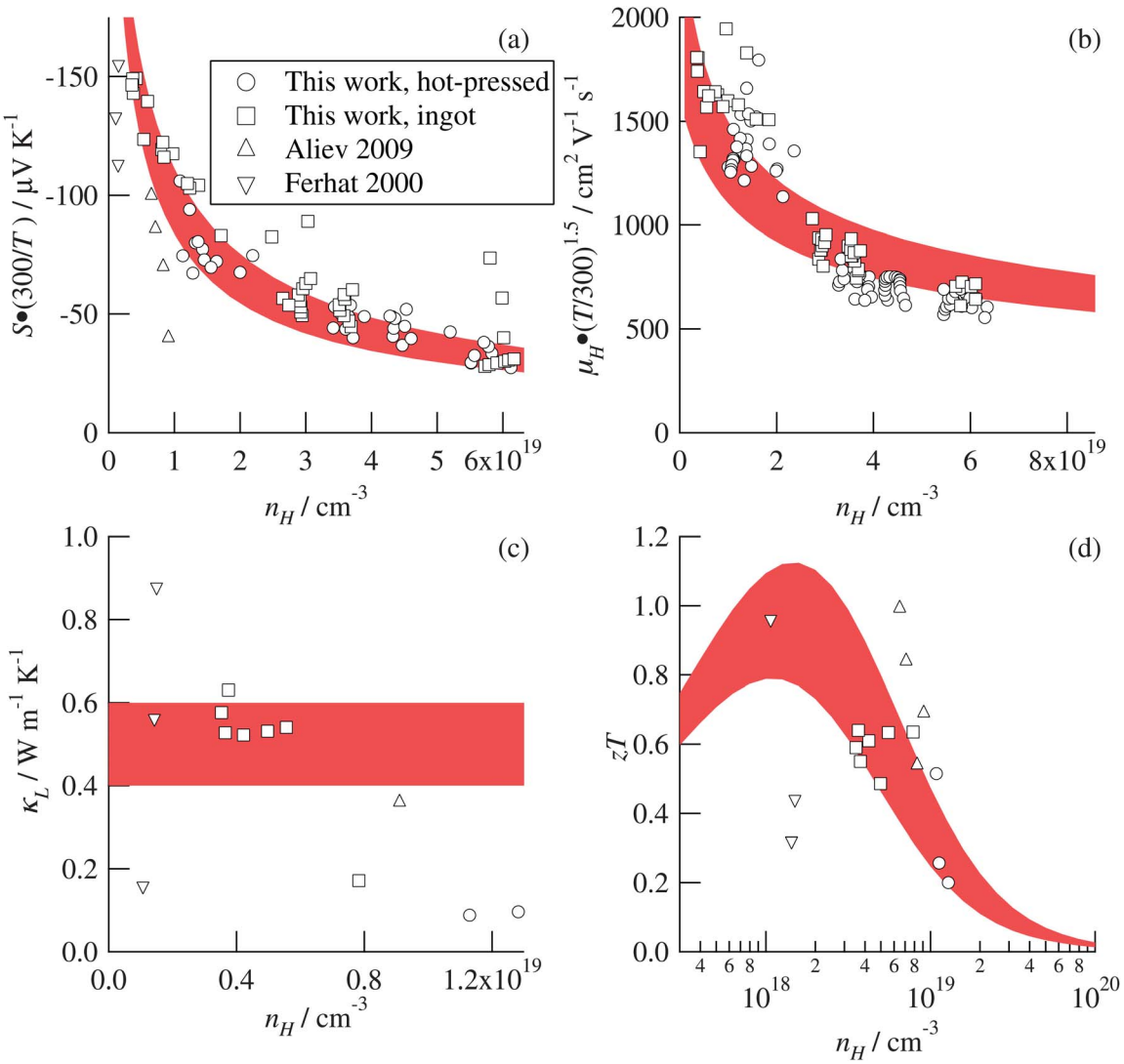

Fig. 2 Estimation of m^*, μ_0, κ_l, and zT as a function of n_H at 300 K. Symbols have the same meaning as in Fig. 1. The Hall mobility values from Ferhat[6] and Aliev[7] were not included in (b) because they are much greater than those obtained in this study. The red bands are predicted curves with the following parameters: (a) upper bound: $m^* = 0.3\ m_e$, lower bound: $m^* = 0.2\ m_e$, (b) upper bound: $\mu_0 = 2800$ cm^2 V^{-1} s^{-1}, lower bound: $\mu_0 = 1800$ cm^2 V^{-1} s^{-1}, (c) $\kappa_l = 0.5$ W m^{-1} K^{-1} ±20%, (d) upper bound: zT computed with parameters for T above phase transition and $\kappa_l = 0.4$, lower bound: zT computed with parameters for T below phase transition and $\kappa_l = 0.6$.

resistivity, since κ_l should decrease with temperature. Above the phase transition, κ decreases slightly with temperature. This is driven by the increase in resistivity in this region.

The lattice thermal conductivity κ_l was estimated from samples with the smallest electronic contribution to be 0.5 W m^{-1} K^{-1} ±20% from the total thermal conductivity data, the resistivity data, and the Lorenz number as determined by the SPB model. The calculated Lorenz numbers are all within 10% of 1.8×10^{-8} V^2 K^{-2}. The calculated lattice thermal conductivities are shown in Fig. 2(c), along with those calculated from previous reports.[6,7]

After estimating the values of m^*, μ_0, and κ_l, we proceeded to estimate zT as a function of n_H at 300 K. Our prediction is shown in Fig. 2(d). The model predicts a zT of 1.1 at a Hall carrier concentration of 1.6×10^{18} cm^{-3}; the predicted zT decreases rapidly above that concentration. The zT values observed in this study (Fig. 1(f)) vary between 0.2 and 0.7 at 300 K and do not exceed 0.2 above 407 K because their Hall carrier concentrations are close to or greater than 10^{19} cm^{-3}, respectively.

Our model suggests that if the Hall carrier concentration were 1.6×10^{18} cm^{-3} above the phase transition, zT would reach approximately 1.2 at 420 K and 1.3 at 600 K. However, we assumed only a single conduction band, while the increase in Hall carrier concentration in some samples at 600 K (Fig. 1(a)) suggests the presence of minority carriers in the valence band at high temperatures. Therefore we predict a broad zT peak near and above 1 between 420 K and 600 K, followed by a decrease in zT at higher temperatures.

The low carrier concentration in $Ag_{2+x}Se$ makes it challenging to achieve the optimum carrier concentration. Thermoelectric materials typically have optimum carrier concentrations in the middle 10^{19} cm^{-3} to the high 10^{20} cm^{-3} range. For example, I-doped PbTe exhibits a maximum zT at 2.9×10^{19} cm^{-3},[16] and Te-doped Bi_2Te_3 has a maximum zT at

2.3×10^{19} cm^{-3}.[19] N-type $CoSb_3$ has an optimum carrier concentration of 1.4×10^{20} cm^{-3} [18] and $La_{3-x}Te_4$ has an optimum carrier concentration of 9×10^{20} cm^{-3}.[17] These carrier concentrations are within the range that can be easily controlled by doping. If a composition of silver, selenium, and a third element with a Hall carrier concentration near the predicted optimum could be found, as in the bismuth antimony telluride solid solutions,[20] it may be possible to achieve a zT greater than 1.

3 Conclusions

We have measured the Hall carrier concentration, Seebeck coefficient, resistivity, and thermal conductivity of $Ag_{2+x}Se$ from 300 K to 673 K, a temperature range never before explored for this material. Additionally, we have successfully used a single parabolic band model to explain the trends in the transport properties with temperature and Hall carrier concentration, and to calculate the effective mass, mobility parameter, and lattice thermal conductivity. Our model suggests that the zT of this material is determined by the Hall carrier concentration and that a zT greater than 1 from 300 K to 600 K can be achieved if the Hall carrier concentration can be reduced to 1.6×10^{18} cm^{-3}. Hence, we have successfully explained the variation in the previously reported values of the thermoelectric efficiency of this material and have provided a mechanism for optimizing its thermoelectric performance.

4 Experimental

Materials synthesis and processing

Compositions of $Ag_{2+x}Se$ with x equal to 0, 0.0006, and 0.0027 were synthesized. Polycrystalline ingots were prepared by melting Ag (shot, 99.9999% pure, Alfa Aesar, Puratronic) and Se (shot, 99.999% pure, Alfa Aesar, Puratronic) in the desired mass ratios inside fused quartz ampoules evacuated to less than 6×10^{-5} torr. The elements were slowly brought to 1273 K, held at that temperature for 12 hours, cooled to 973 K over three hours, annealed at 973 K for three days, then quenched in water. Disk-shaped samples were cut from the ingots.

The remaining materials were cut into ~6 mm pieces and ball-milled to form powders. The powders were hot-pressed at 973 K and 40 MPa for four hours under flowing argon, then held in the hot press at 673 K and ambient pressure for two hours to relieve any internal stresses.[21] The geometric densities of all samples were greater than 95% of their theoretical values.

Materials characterization

Cu K-alpha X-ray diffractometry (PANalytical XPert Pro and Rigaku MiniFlex) confirmed the hot-pressed samples have the same crystal structure (JCPDS 24-1041) as the previously studied Ag_2Se (Fig. S8†).

Thermoelectric properties measurements

The thermoelectric properties of the samples were measured with custom-built and commercial apparatus. The thermal diffusivity α was measured with a Netzsch LFA 457 laser flash analysis unit. The total thermal conductivity was calculated from $\kappa = \alpha d C_p$, where d is the geometric density and C_p is the heat capacity. S was measured with a custom-built device[22] and with an ULVAC ZEM-2. The resistivity ρ, the Hall carrier concentration n_H, and the Hall mobility μ_H were measured with a custom-built system using van der Pauw geometry and a 2 T magnetic field. C_p was measured on a Netzsch 200F3 differential scanning calorimeter from 214 K to 530 K. C_p values above 530 K were extrapolated from the available data.

It should be noted that the measurement of the Seebeck coefficient is sensitive to the manner in which the sample temperature was varied during the measurement. The Seebeck coefficient was measured by oscillating the temperatures of the top and bottom of the sample about a constant average temperature and recording the voltage across the sample as a function of the temperature difference. It was found that it is necessary to use two full oscillations about each average temperature in order to obtain Seebeck coefficients that follow the same path upon raising and lowering the average temperature. Details are given in the ESI and in Fig. S6 and S7.†

Analysis

The effective mass m^* was estimated by fitting Eqns. S(1) and S(6)† to Hall carrier concentration and Seebeck data with m^* as a fitting parameter. The mobility parameter μ_0 was estimated by fitting Eqns. S(1) and S(8)† to Hall carrier concentration and Hall mobility data with μ_0 as a fitting parameter. These parameters were estimated separately for data taken above and below 407 K, *i.e.* for Hall carrier concentrations above and below 3×10^{19} cm^{-3}; we assume that the parameters we estimated represent the possible ranges (shown in Fig. 2(a) and (b)) of effective mass and mobility parameter in the material. m^* and μ_0 are usually estimated at each of a set of temperatures. We used an alternative technique to use the data at all temperatures to estimate m^* and μ_0 at a single temperature. In the single parabolic band (SPB) model, the Seebeck coefficient S is proportional to temperature T.[14] To estimate m^* at 300 K, we plotted $S(T) \times 300\ K/T$ *versus* $n_H(T)$, where $S(T)$ is the Seebeck data and the ratio $300\ K/T$ converts each Seebeck datum to the value it would have at 300 K with the same n_H. The Hall mobility is proportional to $T^{-1.5}$ in the SPB model, so we plotted $\mu_H(T) \times (T/300\ K)^{1.5}$ *versus* $n_H(T)$ to obtain the mobility parameter μ_0.

Acknowledgements

The authors would like to thank the US Air Force Office of Scientific Research for supporting this work.

References

1 L. E. Bell, *Science*, 2008, **321**, 1457–1461.
2 A. D. LaLonde, Y. Pei, H. Wang and G. J. Snyder, *Mater. Today*, 2011, **14**, 526–532.
3 K. F. Hsu, S. Loo, F. Guo, W. Chen, J. S. Dyck, C. Uher, T. Hogan, E. K. Polychroniadis and M. G. Kanatzidis, *Science*, 2004, **303**, 818–821.

4 E. A. Skrabek and D. S. Trimmer, in *Thermoelectrics Handbook*, CRC Press, 1995, ch. 22.
5 H. Scherrer and S. Scherrer, in *Thermoelectrics Handbook*, CRC Press, 1995, ch. 19.
6 M. Ferhat and J. Nagao, *J. Appl. Phys.*, 2000, **88**, 813–816.
7 F. Aliev, M. Jafarov and V. Eminova, *Atomic Structure and Nonelectronic Properties of Semiconductors*, 2009, vol. 43, pp. 1013–1015.
8 C. Lee, Y. Park and H. Hashimoto, *J. Appl. Phys.*, 2007, **101**, 024920.
9 T. Sakuma, K. Iida, K. Honma and H. Okazaki, *J. Phys. Soc. Jpn.*, 1977, **43**, 538–543.
10 H. Liu, X. Shi, F. Xu, L. Zhang, W. Zhang, L. Chen, Q. Li, C. Uher, T. Day and G. J. Snyder, *Nat. Mater.*, 2012, **11**, 422–425.
11 F. Gascoin and A. Maignan, *Chem. Mater.*, 2011, **23**, 2510–2513.
12 G. B. Haxel, J. B. Hedrick and G. J. Orris, *Rare Earth Elements—Critical Resources for High Technology*, United States Geological Survey Technical Report Fact Sheet 087-02, 2002.
13 C. M. Fang, R. A. de Groot and G. A. Wiegers, *J. Phys. Chem. Solids*, 2002, **63**, 457–464.
14 A. H. Wilson, *The Theory of Metals*, The Syndics of the Cambridge University Press, 1958.
15 V. I. Fistul, *Heavily Doped Semiconductors*, Plenum Press, 1969.
16 Y. Pei, A. D. LaLonde, H. Wang and G. J. Snyder, *Energy Environ. Sci.*, 2012, **5**, 7963–7969.
17 A. F. May, J. P. Fleurial and G. J. Snyder, *Phys. Rev. B: Condens. Matter Mater. Phys.*, 2008, **8**, 125205.
18 T. Caillat, A. Borschevsky and J. P. Fleurial, *J. Appl. Phys.*, 1996, **80**, 4442–4449.
19 *Thermoelectrics Handbook*, ed. D. M. Rowe, CRC Press, 1995.
20 *Thermoelectrics Handbook: Macro to Nano*, ed. D. M. Rowe, CRC Press, 2006.
21 A. D. LaLonde, T. Ikeda and G. J. Snyder, *Rev. Sci. Instrum.*, 2011, **82**, 025104.
22 S. Iwanaga, E. S. Toberer, A. D. LaLonde and G. J. Snyder, *Rev. Sci. Instrum.*, 2011, **82**, 063905.